ACS APPLIED MATERIALS & INTERFACES

Research Article

Cite This: ACS Appl. Mater. Interfaces 2019, 11, 25524−25534

www.acsami.org

Hierarchically Structured Janus Membrane Surfaces for Enhanced Membrane Distillation Performance

Nick Guan Pin Chew,[†,§,⊥] Yujun Zhang,[†,§,⊥] Kunli Goh,[§] Jia Shin Ho,[§] Rong Xu,[∥] and Rong Wang*[,‡,§]

[†]Interdisciplinary Graduate School and [‡]School of Civil and Environmental Engineering, Nanyang Technological University, Singapore 639798, Singapore

[§]Singapore Membrane Technology Centre, Nanyang Environment and Water Research Institute, Nanyang Technological University, Singapore 637141, Singapore

[∥]School of Chemical and Biomedical Engineering, Nanyang Technological University, Singapore 637459, Singapore

Supporting Information

ABSTRACT: Commercial hydrophobic poly(vinylidene fluoride) (PVDF) membranes are vulnerable to membrane fouling and pore wetting, hampering the use of membrane distillation (MD) for the treatment of surfactant- and oil-containing feed streams. To address these challenges, we designed novel Janus membranes with multilevel roughness to mitigate foulant adhesion and prevent pore wetting. Specifically, fouling- and wetting-resistant Janus MD membranes with hierarchically structured surfaces were tailored via a facile technique that involved oxidant-induced dopamine polymerization followed by in situ immobilization of silver nanoparticles (AgNPs) on commercial PVDF hollow fiber substrates. These membranes demonstrated outstanding antifouling properties and salt rejection performances in comparison to membranes with single-level structures. We ascribed the membranes' excellent performances to the coupled effects of improved surface hydrophilicity and self-healing mechanism brought about by AgNPs. Furthermore, the newly engineered membranes exhibited antibacterial properties in *Bacillus acidicola* solutions as evidenced by clear inhibition zones observed on a confocal laser scanning microscope. The development of hierarchically structured Janus MD membranes with multilevel roughness paves a way to mitigate membrane fouling and pore wetting caused by low-surface-tension feed streams in the MD process.

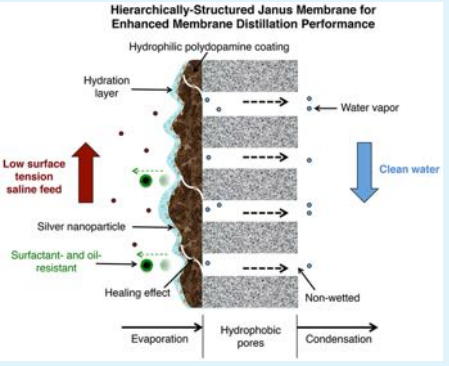

KEYWORDS: *membrane distillation, surfactant, oil, Janus membrane, multilevel hierarchical structure, silver nanoparticle, polydopamine*

1. INTRODUCTION

Membrane distillation (MD) is an emerging separation technique that requires at least one side of a porous membrane to be hydrophobic to inhibit liquid transport.[1] In MD, the temperature gradient across the membrane, which triggers phase changes on and within the membrane structure, drives the separation process.[2] Vapor molecules from the heated feed solution percolate through the hydrophobic membrane pores and condense into pure distillate upon contact with the cooled permeate stream.[3] The competitive advantages of MD over other pressure-driven membrane processes include its low sensitivity to feed salinity and potential utilization of low-grade thermal energy that could lead to relatively lower energy costs.[4]

Surfactants and oils are low-surface-tension contaminants that, even at low concentrations, can reduce the surface or interfacial tension of a medium significantly by adsorbing onto surfaces or assembling at interfaces.[5] These contaminants can adhere readily to the hydrophobic surfaces of traditional MD membranes via hydrophobic and/or electrostatic interactions.[5] This in turn reduces the hydrophobicity and liquid entry pressure of membrane pores, thereby engendering the onset of membrane fouling and pore wetting.[5] Hence, the development of bespoke MD membranes with special wettability is paramount in combating membrane fouling and pore wetting. Janus membranes, "double-sided" membranes with asymmetric wettability on either side of the membrane or at membrane surfaces, hold great potential for water recovery from low-surface-tension feed streams via MD.[6] Fundamentally, these membranes serve as "gatekeepers" between two disparate materials since one side/surface of the membrane is typically lyophilic/hydrophilic, whereas the other is lyophobic/hydrophobic.[7] To endow Janus membranes with asymmetric wettability on opposing sides/surfaces of the membrane, asymmetric surface modification has emerged as the preferred

Received: April 4, 2019
Accepted: June 24, 2019
Published: June 24, 2019

DOI: 10.1021/acsami.9b05967
ACS Appl. Mater. Interfaces 2019, 11, 25524−25534

route in manipulating the surface properties of existing pristine substrates.[8−13]

Polydopamine (PDA) is a bioinspired adhesive that draws its inspiration from mussels' byssus.[14] Its precursor, dopamine, can self-polymerize into PDA at ambient conditions via two synthesis routes to form thin films[15] or primary structures:[12,13] (i) spontaneous autoxidation in slightly alkaline aqueous media by dissolved oxygen[16] and (ii) oxidation in slightly acidic/slightly alkaline aqueous media induced by an oxidant.[17] PDA coatings derive their hydrophilic/superhydrophilic properties from functional groups such as the catechol, quinone, and amine groups, which render PDA an ideal material for the preparation of antifouling membranes.[18] Furthermore, these versatile and material-independent coatings have the ability to adhere to myriads of substrates (wet/dry and/or organic/inorganic) via covalent bonding, hydrogen bonding, π-interactions, metal coordination/chelation, and/or charge-transfer interactions.[18] In particular, the catechol groups present on PDA coatings have the ability to reduce metal ions such as Ag^+ ions through the metal−catechol chelation process via charge transfer for the in situ formation of zero-valent (Ag^0) silver nanoparticles (AgNPs). Furthermore, oxygen- and nitrogen-based ligands on PDA serve as anchor points for the AgNPs to afford secondary hierarchical structures that in turn create a PDA−AgNPs nanohybrid network that contains multilevel hierarchical structures.[19,20]

Previously reported studies have demonstrated the use of PDA and AgNPs to create symmetric surfaces of either enhanced (super)hydrophilicity or (super)hydrophobicity for different membrane applications ranging from pressure-driven reverse osmosis (RO) and ultrafiltration (UF)[19,21,22] to temperature-driven MD processes.[23,24] The objectives included improving membrane performance and operational stability as well as imbuing the membrane surfaces with antifouling and antimicrobial or antiwetting properties. Generally, for MD applications, researchers have hitherto only leveraged on PDA−AgNPs for the creation of rough hierarchical structures on different polymeric materials to achieve superhydrophobicity for antiwetting performance. Liao and co-workers engineered superhydrophobic symmetric MD nanofibers (both feed- and permeate-facing surfaces were superhydrophobic) and ran these membranes in salt solutions during short-term experiments.[23] The biggest critique of this work was the lack of experimental data for low-surface-tension feed streams during long-term operations, which was the main focus of our current work. In a separate study, An et al. designed another type of superhydrophobic symmetric membranes for MD applications that demonstrated relatively good performances in low-concentration oil and surfactant solutions.[25] It is worth noting that the oil solutions used in this study were not emulsified by any surfactant and hence represented an inaccurate way of validating the membranes' antifouling and antiwetting properties. This study would have been of more value had the authors used higher concentrations of low-surface-tension feed streams that simulated actual feed streams found in the industry. Moreover, in both studies, antimicrobial properties were found wanting in these novel symmetric MD membranes that contained PDA−AgNPs nanohybrid networks. On the other hand, in the field of pressure-driven membrane processes, scientists have explored the use of PDA−AgNPs coatings for distinctly different purposes. Huang et al. and Wu et al. tailored symmetric UF membranes, whereas Yang et al. developed symmetric RO membranes that all acquired improved hydrophilicity and demonstrated antimicrobial properties against bacteria such as *Escherichia coli* and *Bacillus subtilis*.[19,21,22] Furthermore, these studies observed enhanced permeation flux along with fouling-resistant properties while maintaining an excellent rejection rate. Adequate evidence was also provided to vindicate the stability of immobilized AgNPs for different membrane processes. Existing PDA−AgNPs designs developed and adopted for pressure-driven membrane processes have provided useful insights into how controlled hydrophilization of hydrophobic MD membrane surfaces could potentially achieve coupled fouling- and wetting-resistant properties as well as long-term operational stability in our mission to recover water from low-surface-tension feed streams via MD.

Improving on these well-established symmetric membrane designs, herein, we demonstrated robust asymmetric Janus membranes for further enhancements in MD applications. Specifically, Janus MD membranes were designed and synthesized with tailored layers of hierarchically structured PDA−AgNPs nanohybrid networks on the outer surfaces of commercial poly(vinylidene fluoride) (PVDF) hollow fiber membranes. A primary-level structure for our Janus membranes was created by leveraging on the desirable properties of PDA coatings. The secondary-level structure was created by AgNPs, which were employed due to their strong and broad-spectrum antimicrobial properties.[26] It is well acknowledged that the amount of water molecules attracted to a hydrophilic surface depends on its surface roughness.[27] As such, we hypothesized that the formation of multilevel hierarchical structures created a larger percentage of solid−liquid interfaces on the lyophilic face of Janus membranes, which in turn formed a stable interfacial hydration layer that endowed the membranes with fouling-resistant properties.[12,13] In this study, the surface chemistry and structure of the newly engineered Janus membranes were investigated comprehensively through a vast array of characterization techniques. The fouling and wetting propensities of the bespoke Janus membranes were studied systematically in a bench-scale direct-contact membrane distillation (DCMD) test rig by feeding a series of low-surface-tension saline solutions that bore minimal charges. These solutions were chosen to eliminate the effects of electrostatic interactions between the model foulants and membrane surfaces. We then compared the performances of these membranes against those of pristine PVDF membranes as well as Janus membranes with single-level structures. The antibacterial effects of AgNPs on the newly developed Janus membranes were demonstrated by evaluating bacteria adhesion and growth via bench-scale tests using *Bacillus* sp. BF1 strain as the model bacterium. Additionally, the stability of AgNPs immobilized on the Janus MD membranes was evidenced by a leaching test during a 24 h DCMD operation. To the best of our knowledge, this is the first report involving the use of hierarchically structured Janus membranes with fouling- and wetting-resistant properties for water recovery from low-surface-tension feed streams via DCMD.

2. MATERIALS AND METHODS

2.1. Materials and Chemicals. Dopamine hydrochloride (DA), sodium periodate (SP), sodium hydroxide (NaOH), nitric acid (HNO_3, 70%), and petroleum (~18% aromatics basis, boiling point 453−493 K) were procured from Sigma-Aldrich (Singapore). Hydrochloric acid (HCl, fuming 37%), sodium chloride (NaCl, 99.5%), anhydrous sodium acetate, 2-propanol (IPA), silver nitrate

DOI: 10.1021/acsami.9b05967
ACS Appl. Mater. Interfaces 2019, 11, 25524−25534

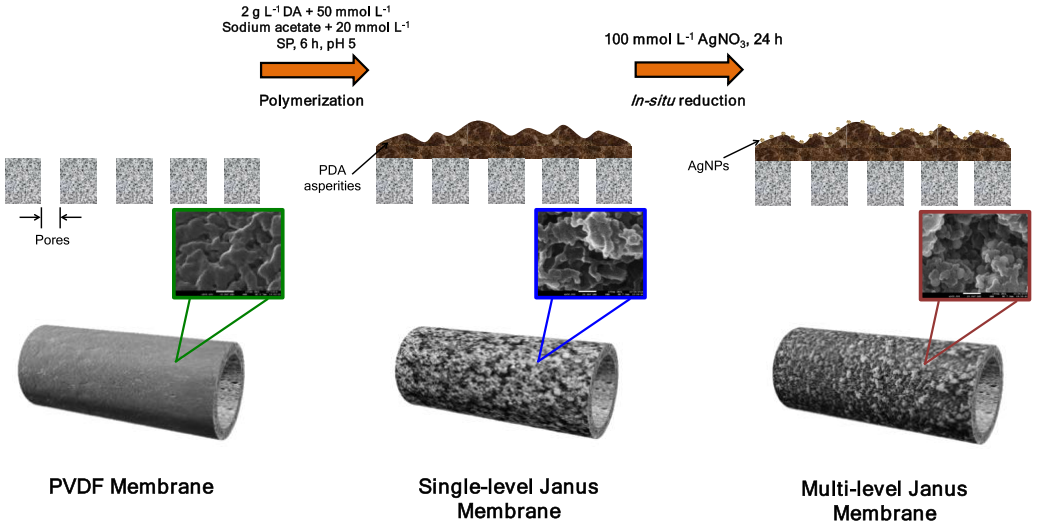

Figure 1. Schematic illustration of the engineering of Janus membranes with multilevel hierarchical structures via oxidant-induced dopamine polymerization and in situ immobilization of silver nanoparticles.

($AgNO_3$), and polyoxyethylenesorbitan monolaurate (Tween 20) were procured from Merck Millipore (Singapore). All procured chemicals and reagents were used as received. Hydrophobic PVDF hollow fiber membranes provided by a commercial supplier were used as substrates for subsequent surface modification and as references for DCMD performance tests. The received membranes were washed and dried through a series of post-treatment steps prior to use as described in our previous works, in which their relevant properties have also been reported.[5,12,13] All aqueous feed solutions and coating solutions were prepared with ultrapure water (Milli-Q water) produced by the Milli-Q Integral Water Purification System (Merck Millipore) and had a resistivity value of 18.2 MΩ cm and a total organic carbon (TOC) value of 3 ppb at 298 K.

2.2. Fabrication of Janus Membranes with Single-Level and Multilevel Hierarchical Structures. The detailed preparation steps involved in the fabrication of Janus membranes with single-level structures have been reported in our previous work.[13] As illustrated in Figure 1, in essence, 2 g L^{-1} DA was stirred homogenously in 50 mmol L^{-1} sodium acetate buffer solution. Following which, 20 mmol L^{-1} SP was added into the mixture. HCl (2 mol L^{-1}) was then added dropwise to adjust the pH of the coating solution from 5.6 to a final value of 5. Prior to performing surface modification, the outer surface of each PVDF hollow fiber membrane was prewetted with a predetermined concentration of IPA for a fixed amount of time and then rinsed thoroughly with Milli-Q water. Subsequently, the pristine PVDF hollow fiber membranes were immersed in the coating solution for 2 and 6 h in an anoxic environment. Hereon, these Janus membranes with single-level structures that were coated for 2 and 6 h will be known as the 2h-S-mPVDF and 6h-S-mPVDF membranes, respectively. Finally, the coated fibers were dried overnight in an oven at 333 K after rinsing them repeatedly with Milli-Q water. On the other hand, to create multilevel hierarchical structures on Janus membranes, the 2h-S-mPVDF and 6h-S-mPVDF membranes were deposited with AgNPs by immersing them in 100 mmol L^{-1} $AgNO_3$ solution for 24 h under ambient conditions in a dark environment since $AgNO_3$ is sensitive to light. These Janus membranes with multilevel hierarchical structures will be hereon denoted 2h-M-mPVDF and 6h-M-mPVDF membranes. Thereafter, the membranes were rinsed thoroughly with Milli-Q water and dried overnight in an oven. The dried hollow fiber membranes were cut to an appropriate length and sealed in lab-scale modules with epoxy resin on both ends. Fresh modules were prepared for each experiment. The effective membrane area in each module was 0.00346 m^2.

2.3. Membrane Characterizations. The detailed characterization procedures and underlying working principles have been explained in our previous studies.[5,12,13] The outer-surface and cross section morphologies of the pristine PVDF, 6h-S-mPVDF, 6h-M-mPVDF, ultrasonicated 6h-M-mPVDF, and 2h-M-mPVDF membranes were observed at different magnifications via a field emission scanning electron microscope (FESEM) (JSM-7200F, JEOL, Japan). The elemental compositions of the 6h-M-mPVDF and ultrasonicated 6h-M-mPVDF membranes were detected via energy-dispersive X-ray (EDX) analyses in a low vacuum mode at 10 kV. The outer-surface roughness of the respective membranes was captured through an atomic force microscope (XE-100, Park Systems, Republic of Korea). The attenuated total reflectance Fourier transform infrared (ATR-FTIR) spectra of the pristine PVDF, 6h-S-mPVDF, and 6h-M-mPVDF membranes were recorded under ambient conditions within the range of 400−4000 cm^{-1} at a resolution of 4 cm^{-1} on a Shimadzu IR-Prestige-21 machine. The surface ζ-potential on the outer surface of the respective membranes was determined by mounting the samples on an adjustable gap cell (20 mm × 10 mm) and undergoing a series of voltage measurements on an electrokinetic analyzer (SurPASS 3, Anton Paar, Austria). The dynamic water contact angle value of the respective membranes was measured by a tensiometer (DCAT11, DataPhysics, Germany) in accordance with the Wilhelmy's method. Images of the underwater interactions between a petroleum droplet and the different membrane surfaces were captured via the captive bubble method on a goniometer (Contact Angle System OCA 15EC, DataPhysics, Germany). The degrees of wettability on the outer surfaces of the pristine PVDF, 6h-S-mPVDF, and 6h-M-mPVDF membranes were determined via the sessile drop method on the goniometer. The adhesive strength and robustness of the modified layer were evaluated qualitatively with reference to the degree of surface deterioration and intactness after the 6h-M-mPVDF membranes were subjected to ultrasonic treatment for 10 min at a frequency of 37 kHz in an ultrasonic bath (FB 15068, Fisher Scientific).

2.4. DCMD Performance Tests. The fouling- and wetting-resistant properties of the newly developed Janus membranes in a series of highly saline low-surface-tension solutions were observed experimentally via a bench-scale countercurrent DCMD test rig as illustrated in our previous study.[2] The detailed steps for the preparation and characterization of these low-surface-tension solutions have been listed in our previous studies.[5,12,13] The detailed procedures involved in the operation of the test rig have also been described in our previous works.[5,12,13] Briefly, the saline feed and Milli-Q water (permeate) were circulated on the shell side at 0.7 L min^{-1} and in the lumen side at 0.25 L min^{-1}, respectively. The inlet temperatures of the feed and permeate streams were kept constant at 333 and 293 K, respectively. Temporal changes in the amount of permeate collected and the accompanying conductivity were recorded

DOI: 10.1021/acsami.9b05967
ACS Appl. Mater. Interfaces 2019, 11, 25524−25534

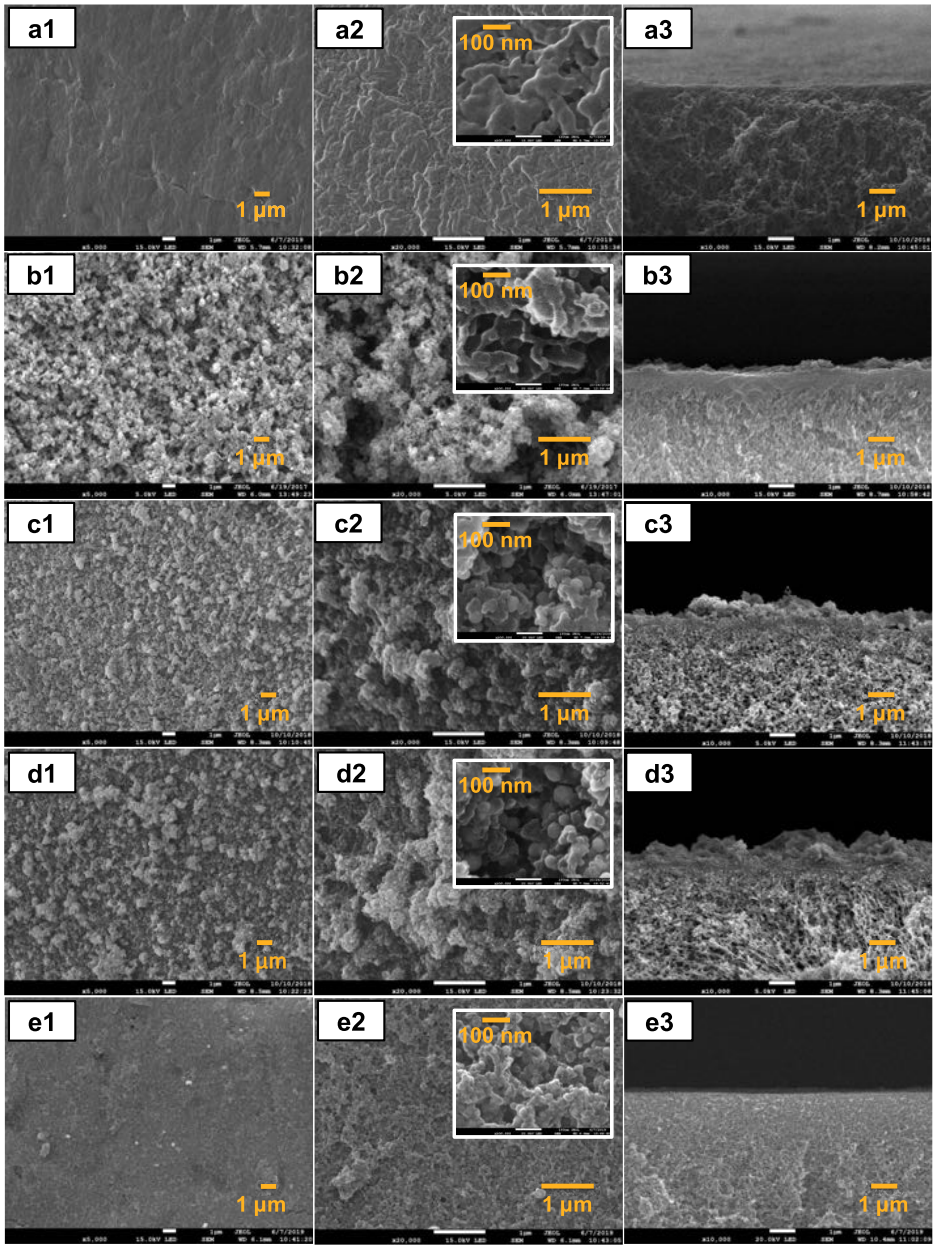

Figure 2. FESEM images of the outer-surface morphologies of the (a1, a2) pristine PVDF, (b1, b2) 6h-S-mPVDF, (c1, c2) 6h-M-mPVDF, (d1, d2) ultrasonicated 6h-M-mPVDF, and (e1, e2) 2h-M-mPVDF membranes. FESEM images of the cross section morphologies of the (a3) pristine PVDF, (b3) 6h-S-mPVDF, (c3) 6h-M-mPVDF, (d3) ultrasonicated 6h-M-mPVDF, and (e3) 2h-M-mPVDF membranes.

at 1 min intervals by the data acquisition system with accuracies of ±0.01 g and ±0.1 μS cm^{-1}, respectively. Each membrane module, as well as other pieces of apparatus of the test rig, was covered with insulation foam to avert further heat loss.

2.5. Antibacterial Assessments. *Bacillus* sp. BF1 strain extracted from a biofouled membrane coupon was used as the model bacterium for antibacterial assessment tests. The membrane coupon was obtained from a bench-scale RO experimental rig used for the treatment of raw seawater from a local desalination plant. Based on 16 S rRNA sequencing results, the strain was identified as *Bacillus acidicola*. The bacterial stock solution was prepared by growing an overnight culture in marine broth (37.4 g L^{-1}) with shaking at 180 rpm at 310 K on an orbital shaker−incubator (ES-20, Biosan, Latvia). Subsequently, the bacteria cells were harvested via centrifugation at 4500 rpm for 20 min at 297 K (Sorvall ST 16 R, Thermo Scientific). Thereafter, the pellets were washed and re-suspended in sterile NaCl solution (0.85%) before sending for centrifugation at 4500 rpm for 10 min at 297 K. This step was repeated once. The concentration of the bacterial stock solution was determined on a flow cytometer (BD Accuri C6 Plus, BD Biosciences, Singapore) for subsequent preparation of feed solutions for antibacterial assessment. Prior to each antibacterial assessment test, the respective membranes were prewetted with IPA and subsequently immersed in Milli-Q water for at least 24 h. Each membrane sample was immersed in 5 mL of bacterial stock solution mixed with 95 mL of marine broth (equivalent to 5 ppm TOC) to achieve a final bacterial concentration of ~4 × 10^6 counts mL^{-1} and shaken at 120 rpm for 120 h at 313 K.

Microscopic observations and image acquisitions of biofilms, or the lack thereof, were captured on a confocal laser scanning microscope (LSM 710, Zeiss, Germany). Prior to that, each membrane sample was stained with LIVE/DEAD BacLight Bacterial Viability Kit (Molecular Probes by Life Technologies, L7012) in accordance with the manufacturer's stipulated protocol. In a word, 15 μL of SYTO 9 green-fluorescent nucleic acid stain and 15 μL of propidium iodide red-fluorescent nucleic acid stain were mixed in 5 mL of buffer solution (0.85% NaCl) to obtain the working solution for staining.

DOI: 10.1021/acsami.9b05967
ACS Appl. Mater. Interfaces 2019, 11, 25524−25534

Each membrane sample was then soaked in the working solution for ~10 min at ambient conditions in the dark. After incubation, the membrane samples were rinsed repeatedly with the buffer solution before being placed on microscope glass slides for confocal observations.

2.6. Silver Loading Quantification and Silver Leaching Test. The total mass of AgNPs immobilized on the 6h-M-mPVDF membrane surfaces was quantified by a dissolution experiment. First, a piece of 6h-M-mPVDF membrane cut to a length of 10 cm was immersed in a test tube filled with 10 mL of 7.2 mol L^{-1} HNO_3 and the membrane was then subjected to ultrasonic treatment for 30 min at a frequency of 37 kHz in an ultrasonic bath. Thereafter, a 20-fold dilution was carried out with Milli-Q water and the dissolved silver concentration was quantified using an inductively coupled plasma optical emission spectrometer (ICP-OES) (Optima 8000, PerkinElmer) with a featured wavelength of 328.068 nm. This experiment was repeated twice, and the mass density of the immobilized AgNPs was tabulated.

The stability of the deposited AgNPs was evaluated by a leaching test conducted on the 6h-M-mPVDF membranes. To simulate the actual operational situation, 50 mL of permeate was collected after a 24 h DCMD operation with 3.5 wt % NaCl as feed solution for concentration measurements using ICP-OES.

3. RESULTS AND DISCUSSION

3.1. Observations of Membrane Surface Morphology. The outer-surface and cross section morphologies of the pristine PVDF, 6h-S-mPVDF, 6h-M-mPVDF, ultrasonicated 6h-M-mPVDF, and 2h-M-mPVDF membranes were captured by FESEM and are presented in Figure 2. The change in the surface morphology of the pristine PVDF membranes after the deposition of primary (PDA) and secondary (AgNPs) levels of hierarchical structures was conspicuous. As observed in Figure 2a1,a2, the pristine PVDF membranes had a relatively smooth and porous outer surface. Triggered by an oxidant, the self-polymerization of dopamine deposited a layer of PDA asperities over the porous pristine PVDF membrane surface after 6 h of reaction time (Figure 2b1−b3). The thin layer of PDA asperities agglomerated to form the primary structures on the newly tailored Janus membranes with relatively high surface roughness as substantiated by the roughness data presented in Table 1. According to the Wenzel theory, the creation of hierarchical structures amplifies the hydrophilicity of a hydrophilic surface.[27] The Wenzel equation for rough hydrophilic surfaces with single-level structures can be written as follows

$$\cos \theta_W = r \cos \theta_Y \quad (1)$$

where θ_W is the apparent contact angle on a surface with single-level roughness, r is the roughness ratio of the actual membrane surface area to the projected area of the membrane surface (r is always >1), and θ_Y is the intrinsic contact angle.

Table 1. Surface Roughness Parameters and Dynamic Water Contact Angle Values of the Pristine PVDF, 6h-S-mPVDF, and 6h-M-mPVDF Membranes

	roughness parameters		
membrane	R_a[a] (nm)	R_z[b] (nm)	water contact angle (deg)
PVDF	21.7	191.5	109.5 ± 1.2
6h-S-mPVDF	113.0	895.9	13.2 ± 2.4
6h-M-mPVDF	147.1	993.0	7.6 ± 4.1

[a]Average roughness. [b]Ten-point average roughness.

In contrast, as seen in Figure 2c1,c2, subsequent immersion of the 6h-S-mPVDF membranes in $AgNO_3$ solution deposited copious amounts of AgNPs on the PDA asperities. These AgNPs were well dispersed as corroborated by EDX analyses presented in Figure 3a and served as secondary structures in the engineering of Janus membranes with multilevel hierarchical structures (6h-M-mPVDF). As substantiated by surface roughness data, constructing secondary hierarchical structures on Janus membranes can further roughen the membrane surface (Table 1). To rationalize this fact, the Wenzel equation can be further modified for rough hydrophilic surfaces with multilevel hierarchical structures[28]

$$\cos \theta_{WW} = r^m r^n \cos \theta_Y \quad (2)$$

where θ_{WW} is the apparent contact angle on a surface with multilevel roughness, r^m is the roughness ratio for microscale (PDA) hierarchical structures, r^n is the roughness ratio for nanoscale (AgNPs) hierarchical structures, and θ_Y is the intrinsic contact angle. Since r is always >1, the modified Wenzel model vindicates that the creation of secondary hierarchical structures can further enhance the hydrophilicity of an intrinsically hydrophilic surface. In asymmetric surface modification, prewetting of pristine substrates in a controlled manner is especially important in preventing wicking or complete hydrophilization of the hydrophobic membrane pores. Here, as observed in Figure 2b3,c3, we managed to keep at least one side of the Janus membranes hydrophobic for vapor transport by taking precautions in ensuring that the coating solution did not penetrate into the bulk of the pristine PVDF substrates. More importantly, the 6h-M-mPVDF membranes possessed superior structural stability as evidenced by minimal changes in the membrane surface morphology (Figure 2d1−d3). In addition, elemental EDX mappings of the 6h-M-mPVDF membranes conducted before and after ultrasonic treatment (Figure 3a1,b1) revealed the presence of elements of interest such as carbon (Figure 3a2,b2), oxygen (Figure 3a3,b3), and silver (Figure 3a4,b4). In particular, the robustness of the AgNPs was validated by the abundance of silver elements that remained on the membrane surface (Figure 3b4) after 10 min of ultrasonic treatment.

3.2. Characterizations of Membrane Surface Chemistry. The ATR-FTIR spectra of the pristine PVDF, 6h-S-mPVDF, and 6h-M-mPVDF membranes are presented in Figure 4, which provided further confirmation on the successful modification of the pristine PVDF membranes and important insights into tailoring of targeted functional groups on the surfaces of the modified membranes. The spectra were recorded in regions where the characteristic transmittance encompasses the disparate functional groups present on the outer surface of the respective membranes. Four unique absorption peaks typically attributed to PDA were observed on both Janus membranes (6h-S-mPVDF and 6h-M-mPVDF) but not on the pristine PVDF membranes. The characteristic bands observed at 1508, 1606, 1701, and 3000−3600 cm^{-1} could be ascribed to N−H bending vibrations, C═C aromatic stretching vibrations, C═O stretching vibrations, and O−H and N−H stretching vibrations, respectively.[13] Both Janus membranes had similar characteristic bands but different peak intensities that could be attributed to the AgNPs core.[29] The ATR-FTIR results were indicative of the successful in situ immobilization of AgNPs on the PDA layer.

While the surface charge property of the respective membranes played no role in the fouling and wetting

DOI: 10.1021/acsami.9b05967
ACS Appl. Mater. Interfaces 2019, 11, 25524−25534

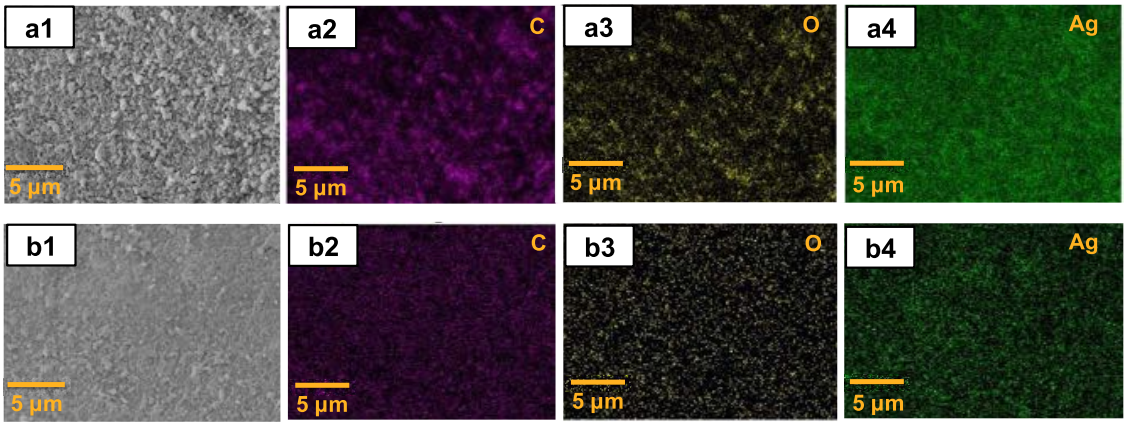

Figure 3. Outer-surface FESEM images and elemental EDX mappings of the respective membranes: (a1−a4) 6h-M-mPVDF and (b1−b4) ultrasonicated 6h-M-mPVDF membranes.

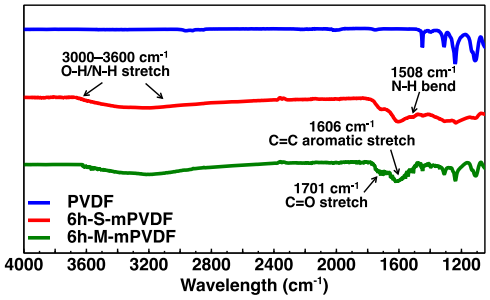

Figure 4. ATR-FTIR spectra of the outer surface of the pristine PVDF, 6h-S-mPVDF, and 6h-M-mPVDF membranes. Transmittance was normalized against the C−F peak. Data for the pristine PVDF and 6h-S-mPVDF membranes were reproduced with permission from (PVDF) ref 5 and (6h-S-mPVDF) ref 13. Copyright (PVDF) 2017 and (6h-S-mPVDF) 2018 Elsevier.

experimental tests conducted in this study, it was still important to determine their surface ζ-potentials to ascertain the effects of the deposition of a PDA layer and AgNPs. As shown in Figure 5, the ζ-potential of each membrane was measured within the pH range of 3−9.5, where protonation or deprotonation of different surface functional groups led to variations in surface ζ-potential along the pH gradient. All

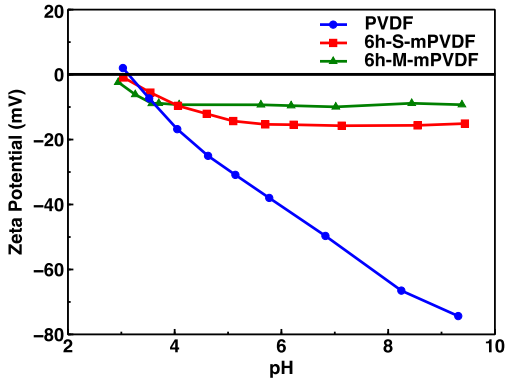

Figure 5. ζ-Potentials of the outer surfaces of the pristine PVDF, 6h-S-mPVDF, and 6h-M-mPVDF membranes as a function of pH. NaCl (1 mmol L^{-1}) was used as the background electrolyte solution. Data for the pristine PVDF and 6h-S-mPVDF membranes were reproduced with permission from ref 13. Copyright 2018 Elsevier.

three membranes were predominantly negatively charged across the tested pH range. However, it was apparent that more negatively charged functional groups were present on the pristine PVDF membrane surface as compared to the two Janus membranes (6h-S-mPVDF and 6h-M-mPVDF), which could be attributed to the electronegative charge of its CF moieties. For both Janus membranes, their surface ζ-potentials decreased gently between pH 3 and 4 before maintaining at a constant value at higher pH values. This observed trend was consistent with other studies on PDA.[11] This could be ascribed to the fact that −NH groups on the PDA layer associated to form $-NH_2^+$ by HCl at lower pH values, whereas the −OH and −COOH groups dissociated to form $-O^-$ and $-COO^-$ by NaOH at higher pH values. The 6h-M-mPVDF membranes were relatively less negatively charged in comparison to the 6h-S-mPVDF membranes since more of their oxygen-containing ligands were affixed with AgNPs.

3.3. In-Air Membrane−Water and Underwater Membrane−Petroleum Interactions. Self-polymerization of dopamine triggered by the oxidant, SP, introduced hydrophilic functional groups such as catechol, quinone, and amine groups. These hydrophilic groups brought about drastic changes to the modified membrane surfaces. The pristine PVDF membranes were intrinsically hydrophobic, presenting an in-air water contact angle value of 109.5 ± 1.2° as listed in Table 1. As observed in Figure 6, the water droplet did not spread across the pristine PVDF membrane surface and remained spherical in shape. In contrast, the deposition of a PDA layer on the 6h-S-mPVDF membranes gave rise to an improved hydrophilicity of 88% (13.2 ± 2.4°) as compared to the pristine PVDF membranes. Figure 6 shows that the tethered water droplet instantaneously spread across the 6h-S-mPVDF membrane surface upon contact, suggesting excellent wettability by water. The deposition of AgNPs on the 6h-M-mPVDF membranes further reduced the in-air water contact angle value to 7.6 ± 4.1°, which translated to a 42% improvement in hydrophilicity in comparison to the 6h-S-mPVDF membranes. This suggests that the addition of AgNPs improved the wettability of membrane surfaces, as corroborated by several other studies.[19,30,31] The captured images of the in-air membrane−water interactions in Figure 6 further validated the improved wettability of the 6h-M-mPVDF membrane surface brought about by the formation of AgNPs via the in situ reduction of Ag^+ by PDA.

DOI: 10.1021/acsami.9b05967
ACS Appl. Mater. Interfaces 2019, 11, 25524−25534

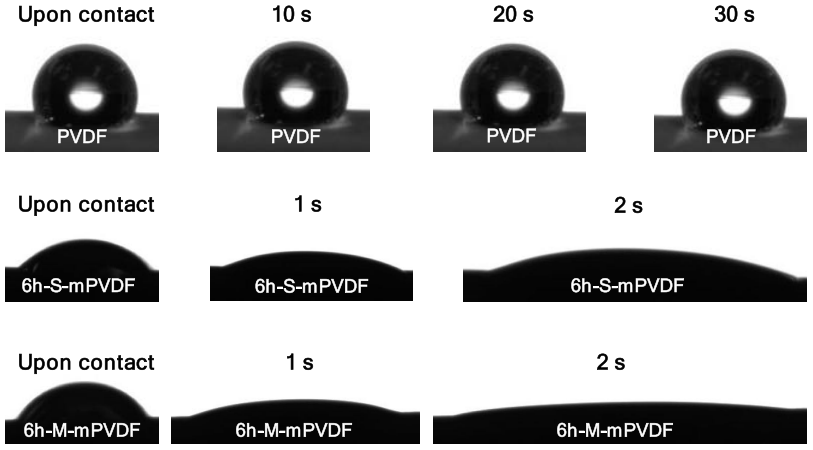

Figure 6. Degree of wettability (1 μL water droplet) on the outer surfaces of the pristine PVDF, 6h-S-mPVDF, and 6h-M-mPVDF membranes.

To obtain relevant insights into the fouling and wetting phenomena caused by petroleum droplets in the subsequent DCMD tests, we captured images of the respective underwater membrane–petroleum interactions via a captive bubble method. A video clip (Video S1) demonstrating the underwater membrane–petroleum interaction between a petroleum droplet and the 6h-M-mPVDF membrane surface has been provided as the Supporting Information. The underwater membrane–petroleum interactions of the pristine PVDF and 6h-S-mPVDF membranes can be found in our previous studies.[12,13] As shown in the captured images presented in Figure 7a1–a3, the pristine PVDF membrane surface exhibited

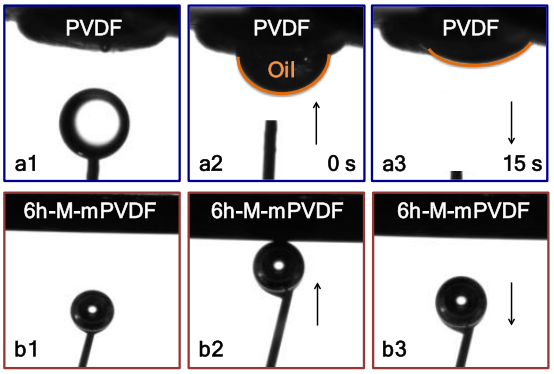

Figure 7. Captured images of the underwater membrane–petroleum interactions. (a1–a3) Pristine PVDF and (b1–b3) 6h-M-mPVDF membranes. Images for the pristine PVDF membranes were reproduced with permission from ref 13. Copyright 2018 Elsevier.

underwater superoleophilic properties. The petroleum droplet readily attached onto the pristine PVDF membrane surface and spread across the membrane surface within 15 s of coming into contact. This suggests that the pristine PVDF membranes would be prone to fouling and wetting by petroleum during the DCMD test. In contrast, it was apparent in Figure 7b1–b3 that the 6h-M-mPVDF membrane surface displayed underwater superoleophobic properties. The petroleum droplet did not adhere to the 6h-M-mPVDF membrane surface despite several forced-contact trials, exhibiting anti-oil-adhesion behavior. This could be attributed to the multilevel roughness and superhydrophilicity contributed by the PDA–AgNPs nanohybrid network. The detailed mechanisms involved in the attractive and repulsive behaviors of the pristine PVDF and modified membranes, respectively, will be discussed in detail in Section 3.4.

3.4. Membrane Performance in DCMD Tests. *3.4.1. Saline Feed with Tween 20.* To investigate the effects of multilevel hierarchical structures on the intrinsic performance of Janus MD membranes, the permeate fluxes and permeate conductivities of the pristine PVDF, 2h-M-mPVDF, and 6h-M-mPVDF membranes were first evaluated by DCMD tests for 24 h with feed solutions containing 3.5 wt % NaCl. Figure 8

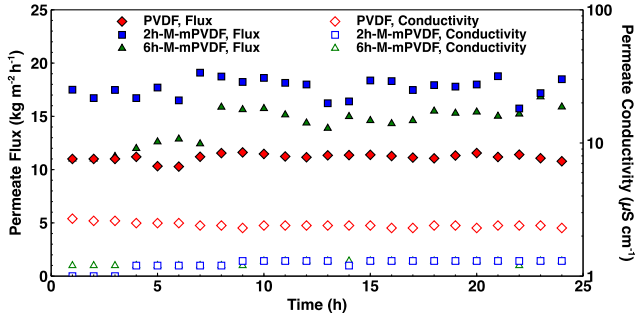

Figure 8. DCMD performances of the pristine PVDF, 2h-M-mPVDF, and 6h-M-mPVDF membranes in 3.5 wt % NaCl solution. Data for the pristine PVDF membranes were reproduced with permission from ref 5. Copyright 2017 Elsevier. [Feed volumetric flow rate (Q_f) = 0.7 L min^{-1}; permeate volumetric flow rate (Q_p) = 0.25 L min^{-1}; feed temperature (T_f) = 333 K; and permeate temperature (T_p) = 293 K.]

illustrates the differences in their respective performances; the permeate flux of the pristine membrane was ~11.16 kg m^{-2} h^{-1}, whereas those of 2h-M-mPVDF and 6h-M-mPVDF membranes were ~17.67 kg m^{-2} h^{-1} (58% enhancement) and ~14.23 kg m^{-2} h^{-1} (27% enhancement), respectively. Both Janus MD membranes showed higher fluxes toward the later stages of the respective tests as compared to the initial stages.

It was hypothesized that the deposited layer on the respective membrane surfaces increased the membranes' resistance to water permeance (and subsequent vapor transport) during the initial stages of the respective experiments when the PDA–AgNPs network had not been fully hydrated by the feed solution. As liquid molecules began to permeate through and fully hydrate the modified surface over time, the resistance was overcome and water molecules were able to pass through it quicker such that the vapor flux could

DOI: 10.1021/acsami.9b05967
ACS Appl. Mater. Interfaces 2019, 11, 25524–25534

reach and maintain at a higher value as the experiments progressed on. Generally, both Janus MD membranes exhibited stable fluxes and conductivities throughout the test duration. This suggests that wicking or hydrophilization of the membrane pores during the modification process was successfully prevented, which kept one side of the Janus membranes hydrophobic for vapor transport and allowed for the complete rejection of nonvolatile NaCl solutes.

In addition, the deposited layer after a specific time of operation did not impede vapor flow across the membrane due to the presence of microridges and valleys as well as possible microdefects on the newly engineered superhydrophilic membrane surfaces that promoted water passage.[19] The enhancement in permeate flux for both Janus membranes could also be ascribed to the excellent wettability of the superhydrophilic coating on their feed-facing surfaces, which assisted in drawing more water molecules to both membrane surfaces as compared to the hydrophobic pristine PVDF membranes. Specifically, the 2h-M-mPVDF membranes collected more permeate than the 6h-M-mPVDF membranes during the test duration, owing to the fact that prolonged membrane modification times yielded a thicker and denser deposited layer (Figure 2c2,c3), whereas shorter modification times yielded a thinner and more porous structure (Figure 2e2,e3). Although kept at an acceptable degree, the thicker deposited layer with more impermeable AgNPs was more likely to block more water pathways within the 6h-M-mPVDF membranes, as evidenced by their relatively lower permeate flux in Figure 8.[19] While the 2h-M-mPVDF membranes exhibited a higher flux than the 6h-M-mPVDF membranes in relatively clean feed solutions that contained only nonvolatile solutes (i.e., NaCl), these membranes have very limited potential for long-term operations in the treatment of surfactant- and oil-containing feed streams due to the unstable interfacial hydration layer ascribed to the lack of distinct hierarchical structures and limited hydrophilicity. In spite of an acceptable compromise on flux, the 6h-M-mPVDF membranes demonstrated comparatively more enduring fouling- and wetting-resistant performances under challenging feed conditions. Therefore, this work focused on the potential of the 6h-M-mPVDF membranes for long-term applications. In the following sections, comparisons were made among these membranes to elucidate the working mechanisms and resulting benefits of depositing multilevel hierarchical structures on Janus MD membranes for treating challenging feed streams containing surfactants and oils.

To explore the impact of the formation of secondary-level structures (AgNPs), long-term DCMD tests were conducted on the pristine PVDF (without hierarchical structures), 6h-S-mPVDF (single-level structures), and 6h-M-mPVDF (multilevel hierarchical structures) membranes. The feed solutions were prepared by adding 50 mg L^{-1} Tween 20 in 3.5 wt % NaCl solutions. Tween 20 is a typical nonionic surfactant that has been widely used in the industry and is present in numerous waste streams. Figure 9 illustrates that the pristine PVDF membranes demonstrated a distinctly abysmal performance as compared to the two Janus membranes, featuring a drastically fluctuant flux accompanied by a rapidly increasing conductivity during the test duration. This was because the pristine PVDF membranes were hydrophobic in nature and the surfactant, a low-surface-tension species, could easily adhere to the membrane surface and pores via hydrophobic interactions. Once attached onto the membrane surface and pores, the

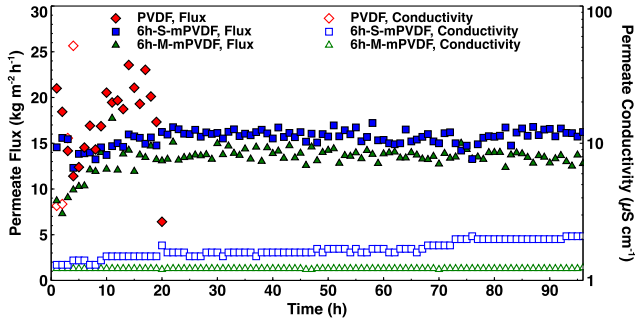

Figure 9. DCMD performances of the pristine PVDF, 6h-S-mPVDF, and 6h-M-mPVDF membranes in 50 mg L^{-1} Tween 20 solution. Data for the pristine PVDF and 6h-S-mPVDF membranes were reproduced with permission from (PVDF) ref 5 and (6h-S-mPVDF) ref 13. Copyright (PVDF) 2017 and (6h-S-mPVDF) 2018 Elsevier. The feed tank was refilled with overflow from the permeate reservoir every 24 h of test duration (Q_f = 0.7 L min^{-1}; Q_p = 0.25 L min^{-1}; T_f = 333 K; and T_p = 293 K).

hydrophilic tails on the Tween 20 unimers began drawing water toward the hydrophilized regions of the pristine PVDF membranes. As a result, the pristine PVDF membranes experienced severe wetting within 20 h of test duration, and NaCl salt in the feed stream diffused through the "broken" barrier that was initially meant for only vapor flow.

In comparison, both Janus membranes with different levels of hierarchical structures exhibited much more stable performances during the test. Both of these membranes were able to maintain low permeate conductivities and sustainable fluxes for 96 h of test duration, demonstrating excellent fouling- and wetting-resistant properties, and most importantly, operational stability. The cause lies in the formation of a stable interfacial hydration layer that spread evenly across the superhydrophilic feed-facing surface and resisted the attachment of low-surface-tension substances.[12,13] Specifically, the Janus membranes with multilevel hierarchical structures (6h-M-mPVDF) presented an even better salt resistance property as indicated by an extremely stable permeate conductivity (steady at 1.3 μS cm^{-1}). On the other hand, the permeate conductivity of the Janus membranes with single-level structures (6h-S-mPVDF) climbed slightly from 1.3 μS cm^{-1} to around 2.1 μS cm^{-1}. The improved wetting-resistant property of the 6h-M-mPVDF membranes was attributed to the deposition of secondary hierarchical structures (AgNPs) with a self-healing function. As described earlier, the formation of PDA asperities rendered the superhydrophilic feed-facing sides of the Janus membranes more permeable to both NaCl solutes and water molecules, whereas the hydrophobic side maintained the membranes' salt rejection property. However, microdefects formed within the PDA layer during the modification process could impair the wetting-resistant property of the 6h-S-mPVDF membranes for the treatment of surfactant-containing feed streams, albeit to a small extent. This rendered the 6h-S-mPVDF membranes slightly more susceptible to the onset of wetting as shown in Figure 9. Interestingly, the in situ immobilization of impermeable AgNPs on these PDA asperities brought about self-healing function that repaired the majority of the microdefects present within the PDA layer.[19] As illustrated in Figure 10, it was hypothesized that during the modification process, these regions of microdefects were accessible to Ag^+ ions in $AgNO_3$ and the formation of localized AgNPs "healed" these defects.[19] This in turn ensured that the salt rejection

DOI: 10.1021/acsami.9b05967
ACS Appl. Mater. Interfaces 2019, 11, 25524−25534

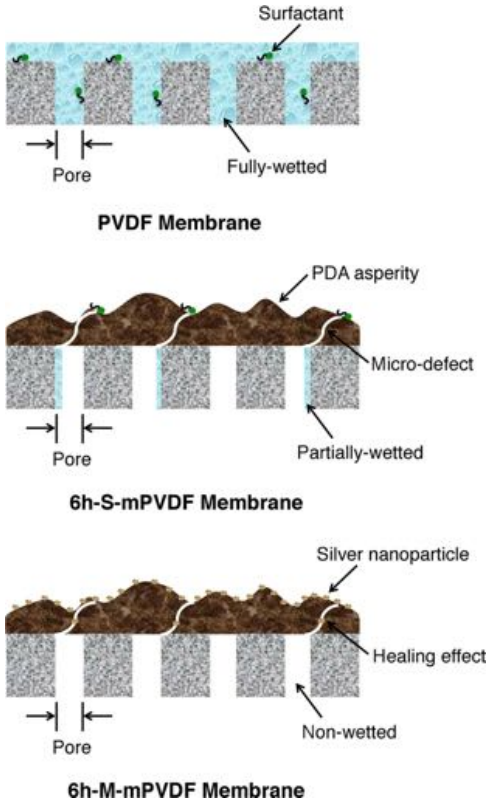

Figure 10. Schematic illustration of the healing mechanism of silver nanoparticles.

property of the 6h-M-mPVDF membranes was sustained throughout the test duration.

3.4.2. Tween 20-Stabilized Petroleum-in-Water Emulsion. To further study the fouling and wetting behaviors of the respective membranes, 500 mg L^{-1} Tween 20-stabilized petroleum-in-water emulsions were prepared as feed solutions. In this feed stream, the competitive advantages of Janus membranes with multilevel hierarchical structures became more apparent. As presented in Figure 11, similar to the results collected in the Tween 20 feed streams, the pristine PVDF membranes experienced severe fouling and wetting within 20 h

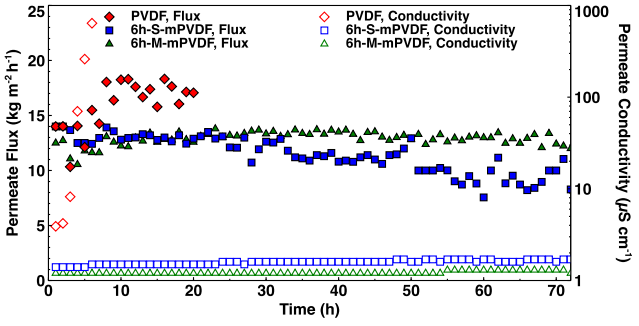

Figure 11. DCMD performances of the pristine PVDF, 6h-S-mPVDF, and 6h-M-mPVDF membranes in a 500 mg L^{-1} Tween 20-stabilized petroleum-in-water emulsion. Data for the pristine PVDF and 6h-S-mPVDF membranes were reproduced with permission from (PVDF) ref 5 and (6h-S-mPVDF) ref 13. Copyright (PVDF) 2017 and (6h-S-mPVDF) 2018 Elsevier. A fresh batch of emulsion was added into the feed tank every 24 h of test duration (Q_f = 0.7 L min^{-1}; Q_p = 0.25 L min^{-1}; T_f = 333 K; and T_p = 293 K).

of test duration because petroleum droplets and Tween 20 unimers present in the emulsion had the tendency to adhere to the superoleophilic feed-facing surfaces of the pristine PVDF membranes ascribed to the effects of hydrophobic interactions. On the other hand, the two Janus membranes showed contrasting fouling behaviors during the test. It can be observed that the Janus membranes with single-level structures (6h-S-mPVDF) showed signs of fouling after 50 h of test duration, as evidenced by the start of gradual flux decline at the 50 h mark. The microdefects within the PDA layer could lead to a slightly less stable interfacial hydration layer, especially at regions where these microdefects were found. As such, some parts of this energetic barrier would have been easily overcome, leading to the accumulative attachment of petroleum droplets and Tween 20 unimers and subsequent pore blockage.

However, when AgNPs were constructed as secondary hierarchical structures, there was a significant improvement in performance. The Janus membranes with multilevel hierarchical structures (6h-M-mPVDF) maintained a stable permeate flux and permeate conductivity (1.3 μS cm^{-1}) during 72 h of test duration. It can be inferred that the presence of secondary hierarchical structures further roughened the membrane surface that in turn enhanced the hydrophilicity of the surface in accordance with the Wenzel model (eq 2). As a result, the interfacial hydration layer could fix more firmly onto the 6h-M-mPVDF membranes' feed-facing surfaces and maintain the strong hydrogen-bonded network to repel potential foulants. Under such a scenario, forces with higher magnitudes (i.e., hydrostatic pressure) were required to overcome this significant energetic barrier. These results demonstrate the potential of engineering multilevel hierarchical structures on Janus MD membranes by endowing these membranes with robust abilities to resist fouling and wetting phenomena, which in turn could lead to sustainable long-term performances in DCMD operations.

3.5. Membrane Antibacterial Behavior in *B. acidicola* Solution. As observed in Figure 12, the antibacterial properties of the respective membranes were ranked as follows: 6h-M-mPVDF (PDA−AgNPs) > 6h-S-mPVDF

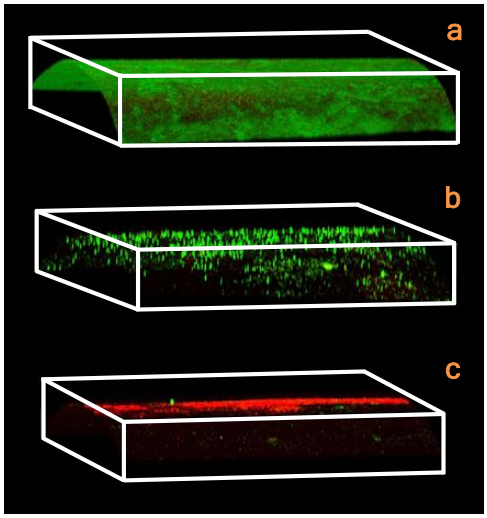

Figure 12. Confocal laser scanning microscopic images of live/dead staining of biofilm on the (a) pristine PVDF, (b) 6h-S-mPVDF, and (c) 6h-M-mPVDF membranes. Live and dead cells are shown in green and red, respectively.

DOI: 10.1021/acsami.9b05967
ACS Appl. Mater. Interfaces 2019, 11, 25524−25534

(PDA) > PVDF. Thick layers of biofilm were observed on the feed-facing surfaces of the pristine PVDF membranes (Figure 12a), whereas clear inhibition zones with negligible amounts of live cells (green) and dead cells (red) were present on the 6h-M-mPVDF membrane surfaces (Figure 12c). AgNPs present on the 6h-M-mPVDF membranes and their released ions annihilated and prevented the proliferation of bacteria cells via direct interaction with sulfur-containing proteins or thiol groups of enzymes that were present within the cells.[21,22] This led to disruption in the electron transport chain and dimerization of DNA.[21] Accordingly, this resulted in shrinking of the cytoplasm and detachment of the cell wall membrane. On the other hand, the 6h-S-mPVDF membranes (Figure 12b) possessed decent antibacterial properties in comparison to 6h-M-mPVDF membranes but a dramatic difference in antibacterial properties when compared against pristine PVDF membranes owing to the much-improved surface hydrophilicity brought about by the deposition of PDA asperities.[21,32] In spite of that, without the presence of AgNPs on the 6h-S-mPVDF membranes, these membranes would be prone to bacterial adhesion and growth in prolonged operations as observed in Figure 12b.

3.6. Stability of Immobilized AgNPs. Based on the ICP-OES test results, the total mass of AgNPs in one membrane module and the mass density of the immobilized AgNPs were calculated to be 2.54 mg and 73.5 μg cm^{-2}, respectively. This provides further evidence that a sufficient number of AgNPs was effectively immobilized on the Janus MD membrane surfaces, which is in good agreement with the FESEM images (Figure 2c1−c3) and elemental EDX mapping results (Figure 3a4).

In addition, the stability of immobilized AgNPs was substantiated by a leaching test conducted on the 6h-M-mPVDF membranes. The mass density of the immobilized AgNPs on the 6h-M-mPVDF membranes after 24 h of the DCMD experiment was tabulated to be 60.4 μg cm^{-2}, which translates to approx. 82.2% of AgNPs that remained on the membrane surfaces. The permeate was collected and measured by ICP-OES after the operation. It is noteworthy to highlight that the silver concentration detected in the permeate stream was lower than the lowest detection limit of the ICP-OES instrument at <0.01 mg L^{-1}. This suggests that the permeate produced by our newly engineered Janus MD membranes was clean and of high quality, considering a silver concentration that was well below the World Health Organization's standard of 0.1 mg L^{-1} and a low salt concentration.[33] Given the adequate amount of AgNPs immobilized on the Janus MD membrane surfaces and the negligible amount of silver detected in the permeate even after prolonged operation, it could be inferred that the in situ immobilization of AgNPs on hierarchically structured Janus MD membranes is a robust technique that ensures operational stability in MD applications.

4. CONCLUSIONS

As a strategy to combat membrane fouling and pore wetting in surfactant- and oil-containing feed streams, novel Janus MD membranes with multilevel hierarchical structures were engineered via oxidant-induced dopamine polymerization followed by in situ immobilization of AgNPs on commercial hydrophobic PVDF hollow fiber membranes. In comparison to membrane surfaces with no hierarchical structures (PVDF) and single-level structures (PDA), the improved surface wettability brought about by multilevel roughness contributed to the newly engineered membranes' robust long-term performances in surfactant solutions and petroleum-in-water emulsions via bench-scale DCMD tests, during which stable fluxes and excellent salt rejection rates were achieved. Depositing multilevel hierarchical structures on Janus MD membranes gave rise to the formation of a stable interfacial hydration layer on the feed-facing surfaces of these membranes and prevented the adhesion of surfactant unimers and petroleum droplets. Furthermore, the antibacterial effects of AgNPs limited the attachment of bacteria cells and subsequent formation of biofilms on the bespoke Janus MD membranes. Silver leaching tests further demonstrated the stability of immobilized AgNPs on these membranes. The results suggest that these novel membranes with excellent fouling- and wetting-resistant properties have the potential for numerous applications via DCMD.

■ ASSOCIATED CONTENT

Supporting Information

The Supporting Information is available free of charge on the ACS Publications website at DOI: 10.1021/acsami.9b05967.

Interaction between an oil droplet and the 6h-M-mPVDF membrane surface (MOV)

■ AUTHOR INFORMATION

Corresponding Author

*E-mail: rwang@ntu.edu.sg. Tel: +65 6790 5327. Fax: +65 6791 0676.

ORCID

Nick Guan Pin Chew: 0000-0001-7634-537X

Rong Xu: 0000-0002-7562-2627

Rong Wang: 0000-0001-8257-0282

Author Contributions

⊥N.G.P.C. and Y.Z. contributed equally to this work and are considered co-first authors.

Author Contributions

The manuscript was written through contributions of all authors. All authors have given approval to the final version of the manuscript.

Notes

The authors declare no competing financial interest.

■ ACKNOWLEDGMENTS

The authors would like to acknowledge funding support from the Singapore Economic Development Board to the Singapore Membrane Technology Centre.

■ REFERENCES

(1) Liao, Y.; Wang, R.; Tian, M.; Qiu, C.; Fane, A. G. Fabrication of Polyvinylidene Fluoride (PVDF) Nanofiber Membranes by Electro-Spinning for Direct Contact Membrane Distillation. *J. Membr. Sci.* **2013**, *425−426*, 30−39.

(2) Yang, X.; Wang, R.; Shi, L.; Fane, A. G.; Debowski, M. Performance Improvement of PVDF Hollow Fiber-Based Membrane Distillation Process. *J. Membr. Sci.* **2011**, *369*, 437−447.

(3) Chen, G.; Yang, X.; Wang, R.; Fane, A. G. Performance Enhancement and Scaling Control with Gas Bubbling in Direct Contact Membrane Distillation. *Desalination* **2013**, *308*, 47−55.

(4) Alkhudhiri, A.; Darwish, N.; Hilal, N. Membrane Distillation: A Comprehensive Review. *Desalination* **2012**, *287*, 2−18.

DOI: 10.1021/acsami.9b05967
ACS Appl. Mater. Interfaces 2019, 11, 25524−25534

(5) Chew, N. G. P.; Zhao, S.; Loh, C. H.; Permogorov, N.; Wang, R. Surfactant Effects on Water Recovery from Produced Water via Direct-Contact Membrane Distillation. *J. Membr. Sci.* **2017**, *528*, 126−134.
(6) Yang, H. C.; Hou, J.; Chen, V.; Xu, Z. K. Janus Membranes: Exploring Duality for Advanced Separation. *Angew. Chem., Int. Ed.* **2016**, *55*, 13398−13407.
(7) Yang, H. C.; Xie, Y.; Hou, J.; Cheetham, A. K.; Chen, V.; Darling, S. B. Janus Membranes: Creating Asymmetry for Energy Efficiency. *Adv. Mater.* **2018**, *30*, No. 1801495.
(8) Zuo, G.; Wang, R. Novel Membrane Surface Modification to Enhance Anti-Oil Fouling Property for Membrane Distillation Application. *J. Membr. Sci.* **2013**, *447*, 26−35.
(9) Lin, P.-J.; Yang, M.-C.; Li, Y.-L.; Chen, J.-H. Prevention of Surfactant Wetting with Agarose Hydrogel Layer for Direct Contact Membrane Distillation Used in Dyeing Wastewater Treatment. *J. Membr. Sci.* **2015**, *475*, 511−520.
(10) Wang, Z.; Hou, D.; Lin, S. Composite Membrane with Underwater-Oleophobic Surface for Anti-Oil-Fouling Membrane Distillation. *Environ. Sci. Technol.* **2016**, *50*, 3866−3874.
(11) Wang, Z.; Jin, J.; Hou, D.; Lin, S. Tailoring Surface Charge and Wetting Property for Robust Oil-Fouling Mitigation in Membrane Distillation. *J. Membr. Sci.* **2016**, *516*, 113−122.
(12) Chew, N. G. P.; Zhao, S.; Malde, C.; Wang, R. Superoleophobic Surface Modification for Robust Membrane Distillation Performance. *J. Membr. Sci.* **2017**, *541*, 162−173.
(13) Chew, N. G. P.; Zhao, S.; Malde, C.; Wang, R. Polyvinylidene Fluoride Membrane Modification via Oxidant-Induced Dopamine Polymerization for Sustainable Direct-Contact Membrane Distillation. *J. Membr. Sci.* **2018**, *563*, 31−42.
(14) Liebscher, J.; Mrowczynski, R.; Scheidt, H. A.; Filip, C.; Haidade, N. D.; Turcu, R.; Bende, A.; Beck, S. Structure of Polydopamine: A Never-Ending Story? *Langmuir* **2013**, *29*, 10539−10548.
(15) Sun, W.; Shen, F.; Wang, Z.; Zhang, Y.; Wan, Y. An Ultrathin, Porous and In-Air Hydrophilic/Underwater Oleophobic Coating Simultaneously Increasing the Flux and Antifouling Property of Membrane for Membrane Distillation. *Desalination* **2018**, *445*, 40−50.
(16) Herlinger, E.; Jameson, R. F.; Linert, W. Spontaneous Autoxidation of Dopamine. *J. Chem. Soc., Perkin Trans. 2* **1995**, 259−263.
(17) Wei, Q.; Zhang, F.; Li, J.; Li, B.; Zhao, C. Oxidant-Induced Dopamine Polymerization for Multifunctional Coatings. *Polym. Chem.* **2010**, *1*, 1430−1433.
(18) Liu, Y.; Ai, K.; Lu, L. Polydopamine and Its Derivative Materials: Synthesis and Promising Applications in Energy, Environmental, and Biomedical Fields. *Chem. Rev.* **2014**, *114*, 5057−5115.
(19) Yang, Z.; Wu, Y.; Wang, J.; Cao, B.; Tang, C. Y. In Situ Reduction of Silver by Polydopamine: A Novel Antimicrobial Modification of a Thin-Film Composite Polyamide Membrane. *Environ. Sci. Technol.* **2016**, *50*, 9543−9550.
(20) Luo, H.; Gu, C.; Zheng, W.; Dai, F.; Wang, X.; Zheng, Z. Facile Synthesis of Novel Size-Controlled Antibacterial Hybrid Spheres Using Silver Nanoparticles Loaded with Poly-Dopamine Spheres. *RSC Adv.* **2015**, *5*, 13470−13477.
(21) Huang, L.; Zhao, S.; Wang, Z.; Wu, J.; Wang, J.; Wang, S. In Situ Immobilization of Silver Nanoparticles for Improving Permeability, Antifouling and Anti-Bacterial Properties of Ultrafiltration Membrane. *J. Membr. Sci.* **2016**, *499*, 269−281.
(22) Wu, H.; Liu, Y.; Huang, J.; Mao, L.; Chen, J.; Li, M. Preparation and Characterization of Antifouling and Antibacterial Polysulfone Ultrafiltration Membranes Incorporated with a Silver-Polydopamine Nanohybrid. *J. Appl. Polym. Sci.* **2018**, *135*, 46430−46439.
(23) Liao, Y.; Wang, R.; Fane, A. G. Engineering Superhydrophobic Surface on Poly(Vinylidene Fluoride) Nanofiber Membranes for Direct Contact Membrane Distillation. *J. Membr. Sci.* **2013**, *440*, 77−87.
(24) Shan, H.; Liu, J.; Li, X.; Li, Y.; Tezel, F. H.; Li, B.; Wang, S. Nanocoated Amphiphobic Membrane for Flux Enhancement and Comprehensive Anti-Fouling Performance in Direct Contact Membrane Distillation. *J. Membr. Sci.* **2018**, *567*, 166−180.
(25) An, X.; Liu, Z.; Hu, Y. Amphiphobic Surface Modification of Electrospun Nanofibrous Membranes for Anti-Wetting Performance in Membrane Distillation. *Desalination* **2018**, *432*, 23−31.
(26) Yang, E.; Chae, K.-J.; Alayande, A. B.; Kim, K.-Y.; Kim, I. S. Concurrent Performance Improvement and Biofouling Mitigation in Osmotic Microbial Fuel Cells Using a Silver Nanoparticle-Polydopamine Coated Forward Osmosis Membrane. *J. Membr. Sci.* **2016**, *513*, 217−225.
(27) Wenzel, R. N. Resistance of Solid Surfaces To Wetting by Water. *Ind. Eng. Chem.* **1936**, *28*, 988−994.
(28) Kim, J.; Choi, S.-O. 11 - Superhydrophobicity. In *Waterproof and Water Repellent Textiles and Clothing*, Williams, J., Ed. Woodhead Publishing, 2018; pp 267−297.
(29) Thota, R.; Ganesh, V. Simple and Facile Preparation of Silver-Polydopamine (Ag-PDA) Core-Shell Nanoparticles for Selective Electrochemical Detection of Cysteine. *RSC Adv.* **2016**, *6*, 49578−49587.
(30) Kim, E.-S.; Hwang, G.; Gamal El-Din, M.; Liu, Y. Development of Nanosilver and Multi-Walled Carbon Nanotubes Thin-Film Nanocomposite Membrane for Enhanced Water Treatment. *J. Membr. Sci.* **2012**, *394-395*, 37−48.
(31) Yin, J.; Deng, B. Polymer-Matrix Nanocomposite Membranes for Water Treatment. *J. Membr. Sci.* **2015**, *479*, 256−275.
(32) Tang, L.; Livi, K. J. T.; Chen, K. L. Polysulfone Membranes Modified with Bioinspired Polydopamine and Silver Nanoparticles Formed in Situ To Mitigate Biofouling. *Environ. Sci. Technol. Lett.* **2015**, *2*, 59−65.
(33) World Health Organization Silver in Drinking-Water. https://www.who.int/water_sanitation_health/dwq/chemicals/silver.pdf (accessed 12 Mar, 2019).

DOI: 10.1021/acsami.9b05967
ACS Appl. Mater. Interfaces 2019, 11, 25524−25534